Volume 4, Issue 3, 2014, 746-753 **ISSN 2069-5837**

Biointerface Research in Applied Chemistry

www.BiointerfaceResearch.com

Original Research Article **Open Access Journal**

Received: 30.11.2013 / Revised: 01.03.2014 / Accepted: 31.03.2014 / Published on-line: 15.06.2014

Preparation and characterisation of manganese and iron compounds as potential control-release foliar fertilizers

Peng Li[1], Yumei Du[2], Li Li[1], Longbin Huang[2], Victor Rudolph[3], Anh V Nguyen[3], Zhi Ping Xu[1,*]

[1]ARC Centre of Excellence for Functional Nanomaterials, The University of Queensland, Brisbane, QLD 4072, Australia
[2]Centre for Mined Land Rehabilitation, The University of Queensland, Brisbane, QLD 4072, Australia
[3] School of Chemical Engineering, The University of Queensland, Brisbane, QLD 4072, Australia

*corresponding author e-mail address:***gordonxu@uq.edu.au***

ABSTRACT

Nanoscale crystals containing manganese and iron as potential foliar fertilizers have been further investigated with the experience accumulated from previous research on potential zinc foliar fertilizer. Compared to Zn(II), Mn(II) and Fe(II) are easily oxidisable in ambient environment, adding stricter criteria to compound selection to prevent oxidation. Adoption of phosphate buffer saline system and chelate have been proposed as the solution and extensively assessed in this paper. After quick co-precipitation, as-prepared crystals were characterised via XRD, FTIR, SEM, TEM, elemental analysis, and AAS to confirm the compositions and two-dimensional nanoscale morphology and assess the nutrient ion release and aqueous stability. In particular, the available Mn concentration in manganese ammonium phosphate and manganese oxalate suspensions was ~10 and ~110 mg/L, respectively. In comparison, ferrous ammonium phosphate and ferrous oxalate suspensions contained ~10 and ~30 mg/L of iron ions, respectively. Therefore, these suspensions can all be used as long-term foliar fertilizers for the correction of Mn and Fe deficiency in plants.

Keywords: *foliar fertilizers, manganese, iron, ammonium phosphate, oxalate, nanocrystals, aqueous solubility, aqueous stability.*

1. INTRODUCTION

Previously we have reported controlled preparation of zinc hydroxide nitrate nanocrystals as potential control-releasing zinc foliar fertilizer, applying concepts and theories from nanotechnology [1]. Here we would like to adopt the accumulated experience to prepare potential manganese and iron control-releasing foliar fertilizers. The desired properties also include nanoscale sheet-like morphology for good leaf adhesion, a suitable aqueous solubility for sustained release, and a long-term stability in ambient environment for a long shelf life. The last itemis more essential in these cases as the plant-preferred Mn(II) and iron(II) can be easily oxidised in ambient environment.

Manganese has been found to be involved in enzyme activation [2], water photolysis [3], lipid metabolism [4], protein synthesis [5], and cell division and extension [6]. Iron is vital to plants for the formation of chloroplasts [7] and ferritins [8, 9], enzyme activation, and protein metabolism [10], and is one of the most essential micronutrients required for the physiological activities of human beings and animals.

Mn-deficient soils distribute widely around the world [11], which is becoming increasingly severe [12] as the bioavailability of the manganese content in soil has not been improved with the supplement of common nutrients [13]. In contrast, iron is the second most abundant metal element on earth. Hence, iron deficiency due to low level of total iron in soils is rare, that in acidic sandy soils in Florida being the most reported example [14]. Loss of bioavailability of iron in soils is the main reason of iron deficiency [15].

"The preceding paper summarises the present state of ignorance rather than knowledge on the subject of manganese fertilizers" [16]. Manganese sulphate [17-20], which was commonly applied in soil applications, has been included in recent achievement of foliar fertilizers as foliar application of plant essential nutrients, particularly micronutrients, is the most effective way to correct nutritional disorder when abiotic constraints inhibit effective nutrient uptake and transport in plants [21]. However, soluble foliar fertilizers are liable to lead to high phytotoxicity when applied at high concentrations, while repeat applications at low concentrations increase the labour cost. To overcome these disadvantages, development of control-releasing foliar fertilizers is necessary. Recently, only some macronutrient control-releasing fertilizers have been reported but applied in soil [22], whereas the micronutrient foliar fertilizers with control-releasing property have been rarely reported.

The major obstacle in the further development of iron fertilizers is the maintenance of the bioavailability of the plant-preferred metastable Fe(II) form. Unlike other micronutrients, only ferrous sulphate has been widely applied as the foliar fertilizer, whereas insoluble iron compounds are yet to become popular in the foliar form. The demand for iron is too high for iron oxides to provide sufficient supply on the leaf surface with a limited area. Hence, development of long-term iron foliar fertilizers with an efficient iron supply could be commercially desirable.

Plant demand [23-25] and toxic tolerance [26,27] of manganese varies with the plant species. Therefore, the potential compounds as control-releasing foliar fertilizers are expected to have multiple options. Manganese ammonium phosphate (MAP) has been reported as a control-release soil fertilizer [28]. Thus it is worth trying to control the size and morphology, and turn it to a

foliar one. Manganese oxalate (MOX) has also been selected as this compound has a relatively higher aqueous solubility, which could be suitable for plants with high Mn tolerance and is reported to exist as the chemical form of Mn in plant leaves [29]. Screening of the iron compounds could refer to the experience from manganese compounds. Ferrous ammonium phosphate [28] (FAP) and ferrous oxalate [30] (FOX) are expected to afford sufficient iron concentration in suspensions, similar to selected manganese compounds.

2. EXPERIMENTAL SECTION

2.1. Sample preparation

Preparation of manganese ammonium phosphate (MAP) or ferrous ammnoum phosphate (FAP) was conducted via precipitation by mixing a solution (50 mL, 0.2M) of manganese sulphate (agricultural grade, Agrichem Co., Ltd, Australia) or ferrous sulphate ($FeSO_4•7H_2O$, ACS reagent, ≥99.0%) with a solution (50 mL, 0.4M) of ammonium phosphate dibasic (ACS reagent, ≥98%, Sigma-Aldrich Co., USA) at 80 °C under vigorous stirring and aged for 1 h. The white or grey green precipitate was collected by filtration, extensively washed with deionised water, and dried at 50 °C for 24h.Solutions of 20 mmol potassium hydroxide (50 mL, reagent grade, 90%, flakes, Sigma-Aldrich Co., USA) and 10 mmol oxalic acid (50 mL, >99%, Sigma-Aldrich Co., USA) were pre-mixed to obtain a solution of potassium oxalate (100 mL, 0.1M). Afterwards, manganese sulphate or ferrous sulphate solution (50 mL 0.2M) was added into freshly prepared potassium oxalate solution at 20 or 80 °C under vigorous overhead stirring, and aged for 1 h. The white or yellow precipitate was collected by filtration, extensively washed by deionised water, and dried at 50 °C for 24h.

2.2. Influence of pH and additives

Citric acid is a common additive in fertilizer preparation but may influence the pH. Unlike Zn^{2+} ion, Mn^{2+} ion can be readily oxidised at high pH and thus lose bioavailability for plant uptake. Though the phosphate solution is a typical buffer system, further investigation on the influence of the additive is necessary. Citric acid and sulphuric acid as additives were added into trisodium phosphate to adjust the pH to approximately 7.2, 8.2, 9.2, 10.2, and 11.2. Manganese sulphate solution was then added into the mixed solution with the initial Mn/P molar ratio of 0.5 at 80 °C under vigorous overhead stirring and aged for 1 h. The pH values after reaction were recorded. The precipitates with white or grey colour were collected by filtration, extensively washed by deionised water, and dried at 50 °C for 24h.

2.3. Aqueous stability and ion release

Approximately 0.5 g of dried solid was added to 50 mL of an aqueous solution with pH of 5.0, 7.0, or 9.0 (adjusted with diluted HNO_3 or NaOH solution), and stirred for 0.5, 1, 3, and 6 h at room temperature. At each time point, the pH value was monitored, and the residual precipitate was collected, washed extensively with deionised water, and dried at 50 °C for 1 day. The samples were stored for 1 month and characterised again by XRD. The aqueous ion release from the precipitate was also examined at room temperature. After grinding, 0.5 g of the dried sample was added to 50 mL of deionised water and shaken for 1 day. The supernatant was collected by filtering with a 0.22 μm filter membrane and subjecting to high-speed centrifugation at 20,000 rpm. Finally, the Mn^{2+} or Fe^{2+} concentration in the supernatant was determined by atomic absorption spectroscopy after adjusting pH to 2 to 3 using diluted HNO_3.

2.4. Characterisation

Powder X-ray diffraction (XRD) patterns were collected using a D8 Advance diffractometer (Bruker AXS Inc., USA) equipped with a copper target, scintillation detector and graphite monochromator with Cu Kα (λ = 1.54Å) radiation. The 2θ angle was scanned at a rate of 1°/min from 5°C to 70°C. The Fourier Transform Infrared (FTIR) spectra were collected in the range of 4000-400 cm^{-1} via FTIR - Attenuated Total Reflectance (ATR) technique in a Nicolet 6700 FTIR spectrometer (Thermo Electron Corp., USA) at a resolution of 2 cm^{-1} for 32 scans. SEM images were recorded in a JEOL JSM-6300 (JEOL Ltd., Tokyo, Japan) to investigate the morphology and the particle size of the samples. The samples were coated by platinum before imaging. JEOL 1010 TEM (JEOL, Tokyo, Japan) was also used for imaging manganese oxalate prepared at 80 °C. An AAnalyst 400 (Perkin Elmer, USA) was employed to determine the cation content released in various solutions. The pH value was monitored by FiveGo pH meter (Mettler-Toledo AG, Switzerland).

3. RESULTS AND DISCUSSION

3.1. Phase composition

The XRD patterns of manganese samples are illustrated in Figure 1. The top two patterns are identified as manganese ammonium phosphate monohydrate ($Mn(NH_4)PO_4•H_2O$, JCPDS card 50-0554, MAP) [31]. The characteristic peaks at 10.1°, 20.3°, 20.8°, 30.5°, 31.5°, 35.7°, 39.1°, 44.1°, 48.0°, 52.0°, and 54.5° correspond to (0 1 0), (0 2 0), (0 1 1), (0 3 0), (1 2 1), (0 3 1), (1 3 1), (1 4 0), (1 4 1), (0 5 0), and (1 5 0) diffractions. The calculated lattice parameters are a = 5.70 Å, b = 8.63 Å, and c = 4.89 Å, respectively, in good agreement with the reported values[31]. In the lower two patterns, the characteristic peaks at 18.0°, 18.2°, 18.6°, 22.4°, 23.9°, 29.4°, 31.2°, 33.2°, 39.6°, 47.4°, and 49.3° correspond to (-1 1 1), (-2 0 2), (2 0 0), (0 0 2), (1 1 1), (-4 0 2), (0 2 0), (1 1 2), (0 2 2), (0 2 3), and (-1 3 1) planes of crystal α-$MnC_2O_4•2H_2O$ (JCPDS card 25-0544, MOX) [32].

Figure 2 shows the FTIR spectra of the manganese samples, indicating similar structural information. The top two spectra correspond well with the reported FTIR spectrum of $Mn(NH_4)PO_4•H_2O$ [31]. Apart from the characteristic peaks attributed to P-O and Mn-O, some peaks for N-H vibrations are also noted. For example, the broad band between 3500 and 2700 cm^{-1} is an overlapped one, and assigned to O-H and N-H stretching vibrations. The peak around 1480 cm^{-1} is attributed to the N-H bending vibration, suggesting the existence of ammonium ions.

Peaks at lower vibrational frequencies (<1200 cm^{-1}) indicate the vibrations due to the P-O and Mn-O bonds.

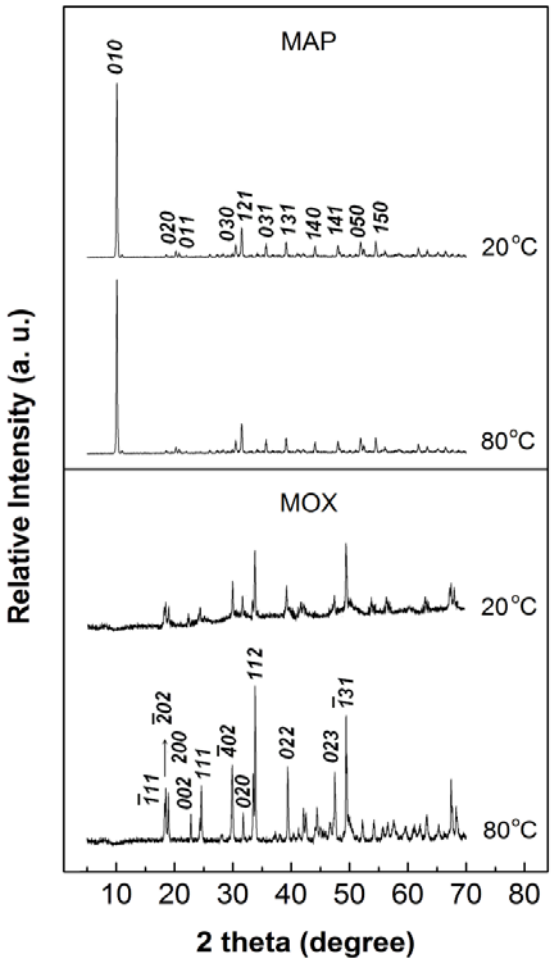

Figure 1. XRD patterns of MAP and MOX.

The lower two FTIR spectra in Figure 2 suggest that the samples are α-MnC_2O_4•$2H_2O$ [33]. The strong and broad band at 3340 cm^{-1} indicates the O-H bonds in the water molecule. The peak due to δ(H_2O) bending apparently is overlapped by the sharp peak at 1625 cm^{-1}, which, together with those at 1360 and 1315 cm^{-1}, is attributed to C-O bonds. The intensive peak around 820 cm^{-1}characterisesδ(O-C-O) + *ν*(C-C) vibrations. The peak at 730 cm^{-1} is assigned to the ρ(H_2O) vibration, while the peak at 605 cm^{-1} illustrates the combined effect of ρ(H_2O) and δring. In addition, the peak at around 490 cm^{-1} represents the vibration of Mn-O bonds [34].

The XRD patterns of the ferrous samples prepared at 20 and 80 °C are shown in Figure 3. The top two patterns show characteristic peaks of ferrous ammonium phosphate (FAP, $Fe(NH_4)(PO_4)$•H_2O, JCPDS card 45-0424). The peaks at 12.0°, 21.8°, 23.7°, 24.6°, 31.8°, and 37.2° correspond to (0 1 0), (1 1 0), (0 2 0), (0 1 1), (1 1 1), and (1 2 1) diffractions of FAP crystals. In addition, peaks observed at ~13.0°, 14.8°, and 17.5° are identified as synthetic maghemite (JCPDS card 25-1402), i.e. Fe_2O_3, corresponding to the diffractions of (1 0 1), (1 0 2), and (1 0 3) planes. The sample prepared at 80 °C seemed to yield better crystals of $Fe(NH_4)(PO_4)$•H_2O. It is noted that the (0 1 0) peak in the FAP pattern at 80 °C has a much higher relative intensity, indicating the preference of crystal growth along with the *b* axis at higher temperatures.

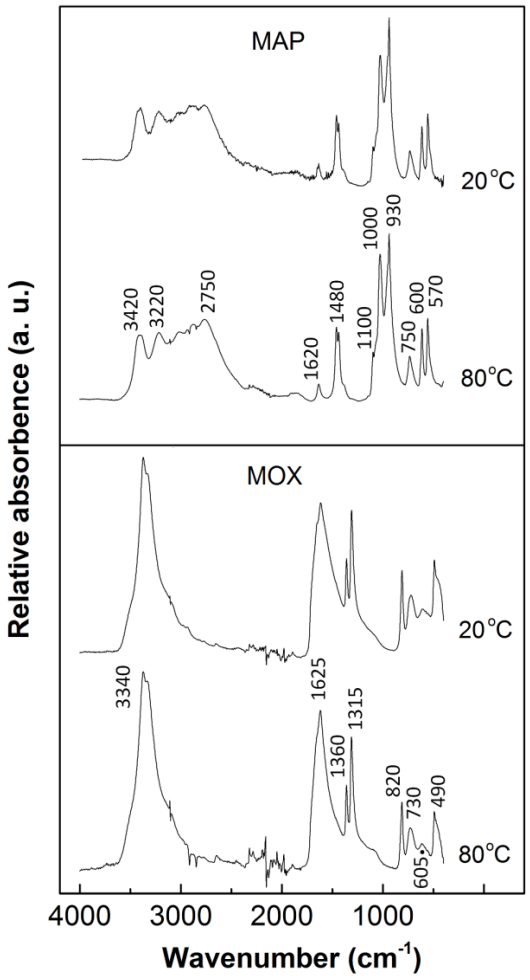

Figure 2. FTIR spectra of MAP and MOX.

The lower two patterns are identified as ferrous oxalate dihydrate (FeC_2O_4•$2H_2O$, synthetic humboldtine, JCPDS card 23-0293, FOX), with the characteristic peaks and the corresponding hkl indices shown in Figure 3. Intensity variation of some peaks was observed, indicating the preference of crystal growth at different ageing temperatures. Careful examination on the XRD peaks indicates that the intensity of peaks of (*h k* 2), including (0 0 2), (-1 1 2), (2 0 2), (-3 1 2), (-2 2 2), (4 0 2), significantly decreased when the temperature was increased from room temperature to 80 °C, revealing the favoured crystal growth along the a and b axes at a higher temperature.

Figure 4 shows the FTIR spectra of FAP and FOX samples. The top two spectra correspond well with the reported IR spectrum of FAP [35]. The broad band between 3500 and 2500 cm^{-1} includes the peak at 3400 cm^{-1} (the O-H stretching vibration of crystal water), the band around 3200 cm^{-1} (the stretching vibration of H-bonded O-H bond), and the band at 3030 cm^{-1} (the stretching vibration of N-H in ammonium group). The small peak at 1640 cm^{-1} is related to the crystal water. The bending vibration of ammonium groups is also observed by the peak at 1430 cm^{-1}. The peaks between 1150 and 960 cm^{-1}characterise the symmetric and asymmetric stretching vibration of P-O bonds in the $[PO_4]^{3-}$ group.

The Fe-O vibration is probably represented by the peaks at 620 and 540 cm^{-1}.

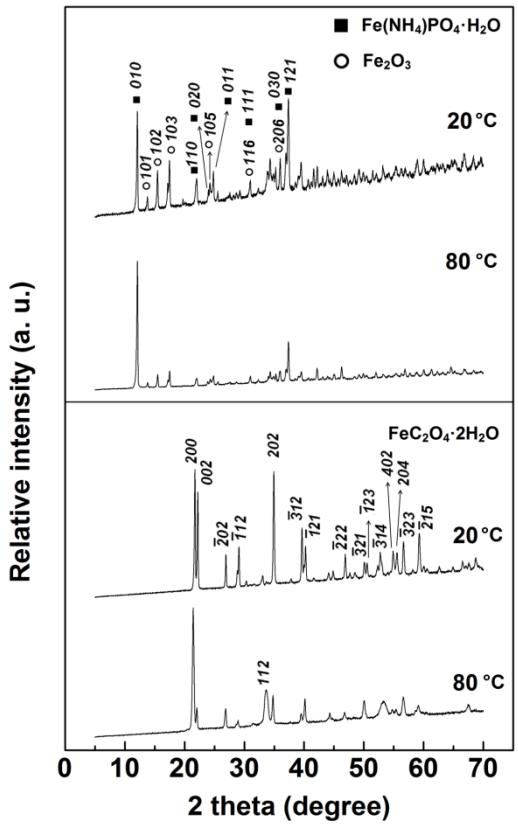

Figure 3. XRD patterns of FAP and FOX.

The lower two spectra confirm that the prepared samples are ferrous oxalate dihydrate. The strong and broad band at 3320 cm^{-1} indicates the O-H bonds in the water molecule. The peaks at 1620, 1360, 1315, and 820 cm^{-1} are respectively attributed to C-O asymmetric stretching, C-O symmetric stretching, O-C-O stretching, and O-C-O bending of oxalate groups [36].

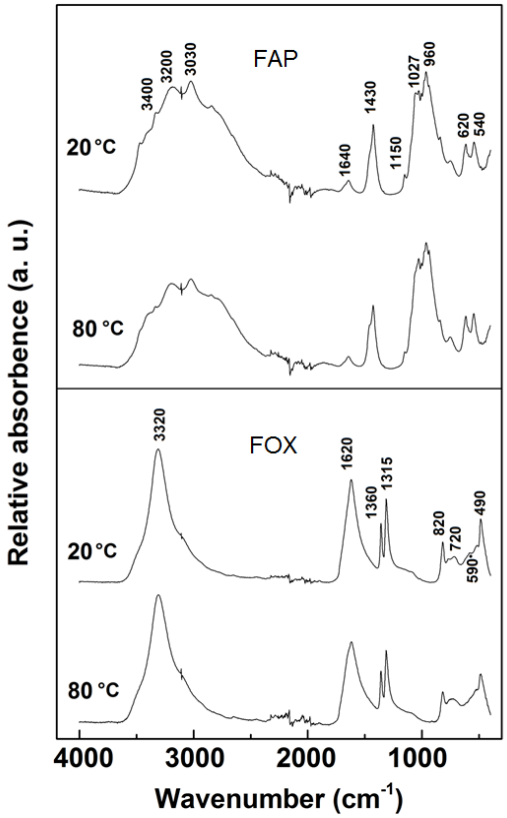

Figure 4. FTIR spectra of FAP and FOX.

The peak at 720 cm^{-1} is assigned to the $\rho(H_2O)$ vibration, while the peak at 590 cm^{-1} illustrates the combined effect of $\rho(H_2O)$ and δ_{ring}. In addition, the peak at 490 cm^{-1} represents the vibration of Fe-O bonds [34].

Table 1. Results of elemental analysis of MAP and FAP. Data represent mean of five independent measures ± standard deviation.

Compounds	N wt. %	Mn or Fe wt. %
MAP ($Mn(NH_4)(PO_4)\cdot H_2O$)	7.53	29.54
MAP 20 °C (Expt)	7.43 ± 0.17	29.83 ± 1.12
MAP 80 °C (Expt)	7.39 ± 0.26	30.01 ± 1.74
FAP ($Fe(NH_4)(PO_4)\cdot H_2O$)	7.49	29.95
FAP 20 °C (Expt)	7.06 ± 0.26	31.17 ± 1.59
FAP 80 °C (Expt)	6.15 ± 0.24	35.45 ± 1.93

Table 2. Results of elemental analysis of MOXand FOX. Data represent mean of five independent measures ± standard deviation.

Compounds	C wt. %	Mn or Fe wt. %
MOX (α-$MnC_2O_4\cdot 2H_2O$)	13.42	30.69
MOX 20 °C (Expt)	13.34 ± 0.26	31.14 ± 1.97
MOX 80 °C (Expt)	13.29 ± 0.20	31.15 ± 2.36
FOX (α-$FeC_2O_4\cdot 2H_2O$)	13.33	31.11
FOX 20 °C (Expt)	13.29 ± 0.44	31.92 ± 2.01
FOX 80 °C (Expt)	13.25 ± 0.72	32.08 ± 1.64

Tables 1 and 2 summarise the wt. % of all samples, measured via CHNS analysis and AAS. The experimental and estimated data of MAP, MOX, and FOX have little differences, suggesting pure phases in these precipitates. Exceptionally, FAP samples have observable lower N contents and higher Fe contents than the theoretical values, in particular for the sample prepared at

80 °C, indicating the existence of ferric oxide impurity, which is in accordance of the results suggested by the XRD pattern (Figure 3).

3.2. Morphology

The SEM images of the MAP samples are shown in Figure 5a and 5b. MAP particles prepared at 80 °C are sheet-like, with the lateral dimension of 1-4 μm and the thickness of 200-500 nm. MAP prepared at room temperature forms bundles of microscale pole-like particles. The shortest dimension is close to 0.5-1 μm.

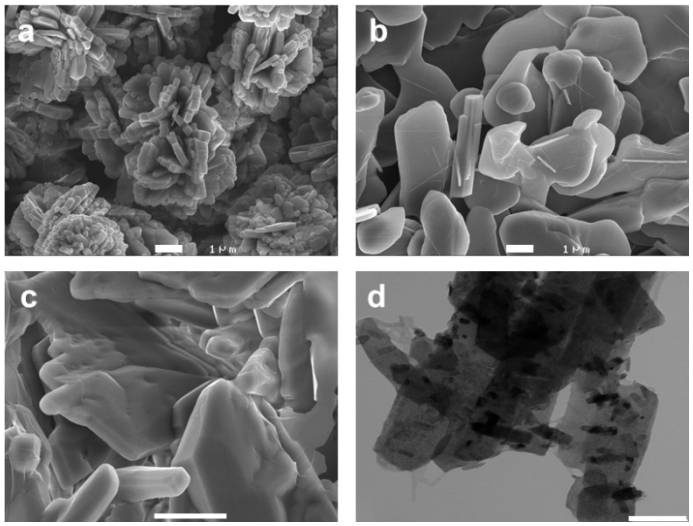

Figure 5. Morphology of MAP prepared at (a) 20 and (b) 80 °C (scale bar = 1 μm) and MOX prepared at (c) 20 (SEM) and (d) 80 °C (TEM) (scale bar = 200 nm)

MOX prepared at 20 °C (Figure 5c) includes microscale particles with a length of 5-10 μm, width of 2-3 μm and thickness of 1 μm. By contrast, MOX prepared at 80 °C (Figure 5d) is too thin to be well characterised by SEM. Thus, TEM image was recorded, which illustrates that the sheet-like particles are approximately 1.5 μm long, 0.5 μm wide and 0.1-0.2 μm thick.

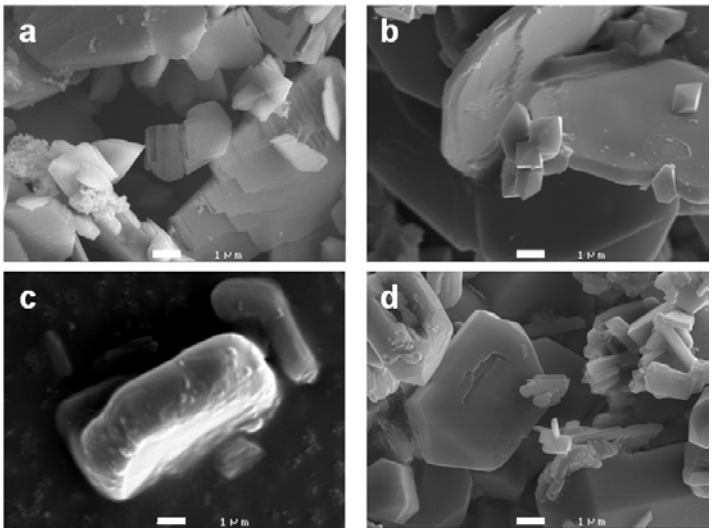

Figure 6. SEM images of FAP prepared at (a) 20 and (b) 80 °C and of FOX prepared at (c) 20 and (d) 80 °C (scale bar = 1 μm)

The morphology of the iron samples are illustrated in Figure 6.Octahedral particles have been observed in Figures 6a and 6b among the large sheet-like particles, confirming the information identified in phase identification, i.e. the samples are a mixture of ferrous ammonium phosphate (sheet-like) and ferric oxide (octahedral). Sheet-like ferrous ammonium phosphate prepared at 80°C seems to have a larger lateral size (~10 μm) than the sample prepared at 20 °C (2-6 μm), whereas the variation of the thickness is little. The preference of the crystal growth along the lateral direction can therefore be illustrated by the comparison of the SEM images as well as the intensities of the (0 1 0) peaks in the XRD patterns.

Figures 6c and 6d show the SEM images of FOX prepared at 20 and 80 °C. The sample prepared at 20 °C has larger aggregates with size over 10 μm, while the sample prepared at 80 °C has various morphologies, from smaller sheet-like to thicker hexagons, with a wide size distribution ranging from 1 to 8 μm.

3.3 Influence of preparation parameters

3.3.1 Influence of temperature

The crystal phases of MAP and MOX prepared at room temperature remained the same as those prepared at 80 °C (Figure 5), but show different morphologies. Both samples prepared at lower temperatures have much larger particles than those prepared at 80 °C. MAP kept its sheet-like morphology, however, significantly aggregated at a lower temperature. Regarding MOX, high temperatures seem to favour nucleation over crystal growth, producing smaller particles. The temperature effect could be well explained by the mechanism proposed by La Mer*et al.* for the formation of colloids or nanocrystals [37]. They suggested that a large number of nuclei form in a short period of time when the concentration of the colloids is beyond the saturation concentration. A higher temperature boosts the nucleation, reducing the concentration of the crystal precursor for following growth and subsequently leading to smaller crystals.

As for iron compounds, the reaction temperature seems to have some impact on the purity of FAP as well as on the particle size (Figure 6). This could be attributed to the oxidation, which would occur faster at a higher temperature and result in some impurity (Table 1). Although Fe_2O_3 was observed in FAP samples prepared at 20 and 80 °C (Figure 3), the composition analysis indicated there was more Fe_2O_3 in the sample prepared at 80 °C. More obviously, FOX sample prepared at 80 °C shows a much regular shape but varied morphology, while preparation at 20 °C gives severe aggregates (Figure 6).

3.3.2 Influence of additives

Table 3 shows the pH values after the reaction between manganese sulphate and sodium phosphate with the initial pH modified to approximately 7.2, 8.2, 9.2, 10.2, and 11.2 with sulphuric or citric acid. The table lists the initial pH and the final pH in two cases. Very interestingly, the precipitate was either white or grey (shaded ones). The grey precipitate means that oxidation occurred, as only black Mn_3O_4 was obtained when sodium phosphate with the pH of ~12.2 was mixed with $MnSO_4$ solution (data not shown). The grey precipitates were apparently the mixture of white hureaulite (data not shown) and black Mn_3O_4.

Based on the final pH and the precipitate colour, it seems that when the final pH is < 7.3-7.5, oxidation does not occur.

When the final pH is > 7.5, e.g. the solution is slightly basic, oxidation takes place:

$$6Mn^{2+} + 12OH^- + O_2 = 2Mn_3O_4\downarrow + 6H_2O \quad (1)$$

It is noted that all final pH values of the citric-modified series are higher than those of the sulphuric-modified ones except for the one under a highly basic condition (initial pH = 11.2).

Table 3.pH variation in reactions from sulphuric- and citric-modified sodium phosphate.

Initial pH	7.20	8.20	9.20	10.20	11.20
Final pH with H_2SO_4 as additive	6.23	6.80	6.95	7.27	9.22
Final pH with citric acid as additive	7.15	7.57	7.68	7.82	9.19

The higher final pH could be due to the particular chelation of citrate with Mn^{2+} ions. Citrate here acts as a tridentate chelate involving the central hydroxyl and carboxyl groups. These groups lie in a plane perpendicular to that of the C(2)-C(3)-C(4) backbone. Such a plane conformation is stabilised by the intramolecular hydrogen bonding between the H atom in hydroxyl group and one O atom in the central carboxyl group [38]. As $\log K_3$ of citric acid is -6.40 [39], the citrate form in all modified solutions should be $[C_6H_5O_7]^{3-}$ only. Formation of manganese citrate complex therefore releases OH^- groups:

$$Mn^{2+} + [C_6H_5O_7]^{3-} + H_2O \leftrightarrow Mn(HC_6H_5O_7) + OH^- \quad (2)$$

The stability constants $\log\beta_1$ of $Mn(HC_6H_5O_7)$ is 3.67 [39].Hence, the chelation leads to a higher final pH, boosting reaction (1).In the exceptional case that the initial pH was 11.2, the final pH value of the citric-modified reaction is similar to that of the sulphuric-modified one because in both suspensions Mn^{2+} was oxidised.

3.4 Aqueous stability

Figure 7 demonstrates the pH variation along the time when samples prepared at 80 °C were added into solutions with the initial pH at 5.0, 7.0, and 9.0. The pH values of the suspensions became steady after 3 h in these cases. Both MAP and FAP suspensions showed a certain buffer capacity, giving weakly basic solutions, whereas MOX showed much less buffering ability, with the final pH depending on the initial pH.

In the MAP and FAP suspensions, MAP and FAP is partially dissolved, as follows:

$$M(NH_4)(PO_4) \leftrightarrow M^{2+} + NH_4^+ + PO_4^{3-} \quad (3)$$

The resultant three ions can all be further hydrolysed, determining the final suspension pH. The hydrolysis of PO_4^{3-} results in more OH^-:

$$PO_4^{3-} + H_2O \leftrightarrow HPO_4^{2-} + OH^- \quad (4)$$

$$HPO_4^{2-} + H_2O \leftrightarrow H_2PO_4^- + OH^- \quad (5)$$

It is well known that HPO_4^{2-} and $H_2PO_4^-$ form a buffer system: phosphate buffer saline. To the contrary, the hydrolysis of M^{2+} and NH_4^+ generates some H^+,

$$NH_4^+ + H_2O \leftrightarrow NH_3{\bullet}H_2O + H^+ \quad (6)$$

$$Mn^{2+}/Fe^{2+} + H_2O \leftrightarrow [Mn/Fe(OH)]^+ + H^+ \quad (7)$$

$$Mn^{2+}/Fe^{2+} + 2H_2O \leftrightarrow [Mn/Fe(OH)_2] + 2H^+ \quad (8)$$

$$Mn^{2+}/Fe^{2+} + 3H_2O \leftrightarrow [Mn/Fe(OH)_3]^- + 3H^+ \quad (9)$$

These reactions will reach an overall equilibrium and determine the dissolution of MAP/FAP and the final pH. In these reactions, hydrolysis of PO_4^{3-} is predominant (pK_{a3} = 12.3), resulting in a basic suspension. In addition, since the complex formation constants ($\log\beta_n$) of $[Fe(OH)]^+$ (5.56) and $[Fe(OH)_3]^-$ (9.67) is larger than those of $[Mn(OH)]^+$ (3.9) and $[Mn(OH)_3]^-$ (8.3), the hydrolysis of Fe^{2+} is more than that of Mn^{2+}, which generates more H^+ and thus leads to a relatively lower final pH (7.9 vs 8.5-8.7 in Figure 7).

On the other hand, the hydrolysis of Fe^{2+} seems (Eqs. 7-9) to be predominant in the process of FOX dissolution and the subsequent overall equilibrium, although $C_2O_4^{2-}$ is also hydrolysed:

$$C_2O_4^{2-} + H_2O \leftrightarrow [HC_2O_4]^- + OH^- \quad (10)$$

Since $C_2O_4^{2-}$ is a much weaker base than PO_4^{3-}, its hydrolysis is very much limited, so the pH is mainly determined by the hydrolysis of Fe^{2+}, to be about 5.7 (Figure 7). In comparison, Mn^{2+} is hydrolysed to a smaller extend, thus the final pH of MOX suspension is varied depending on the initial pH.

Therefore, we propose that the vulnerable chemical stability of Mn(II) and Fe(II) requires either a buffer system or an isolating field (chelate) to prevent oxidation. In this context, MAP, MOX, FAP and FOX prepared in this research were relatively stable, and thus suitable for the uptake by plant leaves as foliar fertilizers. In addition, the XRD patterns of allsamples stored for 1 month do not show any identical variation of crystal phase (data not shown), indicating that these samples are consistent in ambient environment and have good shelf lives.

3.5 Ion release

In addition to the crystal size and morphology, another important property is the ion release capacity of the potential foliar fertilizer. The AAS data in Table 4 show MAP has a Mn^{2+} ion release (~10 mg/L) whereas MOX can afford approximately 110 mg/L of Mn^{2+} ions, which is higher than that an on-sale fertilizer (provided by AgriChem Co. Ltd.) provides (~70 mg/L Mn ions) in suspension. The major component of the industrial fertilizer is manganese carbonate ($\log K_{sp}$ = -9.3). However, the acidic additive significantly boosts the Mn^{2+} release by consuming carbonate and influencing the dissolution equilibrium of manganese carbonate.

As the critical deficiency concentration of manganese in leaf is 10-15 mg/kg dry weight [41], thus the $[Mn^{2+}]$ would be 4-6 mg/L if all Mn^{2+} ions were in the aqueous solution (the average water content in leaf is ~70 wt. %), and subsequently,$[Mn^{2+}]$ in the fertilizer suspension should be more than 4-6 mg/L if the ion diffusion is the main pathway. On the other hand, the critical toxic concentration of manganese is various, depending on the plant species.The common toxic level of Mn^{2+} for crops is ~1,000 mg/kg dry weight [42], i.e. ~300 mg/L in the plant solution if we suppose

all Mn^{2+} ions are in the liquid phase. In this context, MAP and MOX can afford sufficient Mn^{2+} ions and would be suitable tocorrect slight and severe deficiency of Mn^{2+}, respectively.

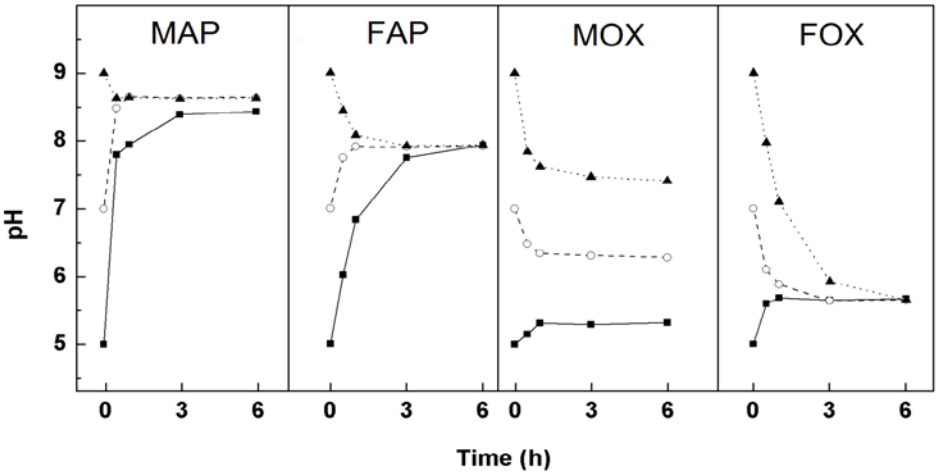

Figure 7.pH variation of solutions with initial pH at 5.0, 7.0, and 9.0 after adding as-prepared samples

Table 4. Ion release from samples prepared at 80 °C. Data represents mean of five independent measures ± standard deviation.

	Compounds	$[M^{2+}]$ (mg/L)	logK_{sp}[39]	Phase composition
Mn	MAP	9.51 ± 0.57	-12.0	$Mn(NH_4)(PO_4)\cdot H_2O$
	MOX	110.56 ± 4.62	-5.3	α-$MnC_2O_4\cdot 2H_2O$
	On-sale Mnfertilizer	68.51 ± 3.71	-9.3	$MnCO_3$ + acidic additive
Fe	Synthetic FAP	8.69 ± 1.33	-10.8[40]	$Fe(NH_4)(PO_4)\cdot H_2O$ + 15~18% Fe_2O_3
	FOX	29.73 ± 2.56	-6.5	α-$FeC_2O_4\cdot 2H_2O$
	On-sale Fe fertilizer	9.69 ± 2.03	--	FeO(OH) + acidic additive

Note: values of K_{sp}areofpure-phase MAP, FAP, MOX, FOX and $MnCO_3$, respectively.

As for iron products, the on-sale iron foliar fertilizer (Agrichem Co., Ltd.) could afford ~10 mg/L iron ions with the assistance of acidic additives. FAP releases approximately 9 mg/L iron ions in the aqueous phase, which is competitive to the commercial one while used in naked FAP suspension. However, the ions released from the on-sale fertilizer (FeO(OH) as major effective component) should be ferric ones, which is less preferred by plants than ferrous ions from FAP. FOX provides much more available iron ions (about 30 mg/L). The Fe^{2+} release from ferrous oxalate is much lower than Mn^{2+} release from manganese oxalate, which is attributed to the lower K_{sp} of ferrous oxalate.

As the critical deficiency and toxic concentrations of iron in plant leaves are 30-50 and 400-1,000 mg/kg dry weight while the average water content in a leaf is ~70% [41], we suggest that the suitable Fe^{2+} concentration in the suspension of long-term foliar fertilizer is 20-150 mg/L. To this end, FOX seems a suitable candidate, while the commercial one and FAP would not efficiently correct the Fe deficiencywithout aid of dissolution.

4. CONCLUSIONS

Ammonium phosphates and oxalates of Mn(II) and Fe(II) were successfully synthesised by co-precipitation under various conditions. Phase identification and microscopic analysis reveal these crystal phases and sheet-like nanoscale morphology of ammonium phosphates and manganese(II) oxalate while ferrous oxalate particles are much thicker. The influences of the preparation parameters including the ageing temperature and additives were investigated systematically. Their aqueous stability and solubility were investigated to evaluate the feasibility as potential long-term foliar fertilizers. All samples in suspensions had a stable pH after 3-h dispersion, and the solid phases wereconsistent. The Mn^{2+}ion release suggests that MAP (~10 m/L) and MOX (~110 mg/L) can be potentially applied as long-term foliar fertilizer for slight and severe cases of Mn deficiency. Correspondingly, ferrous ammonium phosphate and ferrous oxalate can afford ~10 and ~30 mg/L Fe^{2+} in suspensions, respectively, having better performance than on-sale fertilizes, and thereforecould besuitable as potential iron foliar fertilizers.

5. REFERENCES

[1] Li, P., Xu, Z. P., Hampton, M. A., Vu, D. T., Huang, L., Rudolph, V., Nguyen, A. V. Control Preparation of Zinc Hydroxide Nitrate Nanocrystals and Examination of the Chemical and Structural Stability. *J. Phys. Chem. C*, 116, 10325-10332, **2012**.

[2] Hochman, Y., Carmeli, C. Correlation Between the Kinetics of Activation and Inhibition of ATPase Activity by Divalent Metal Ions and the Binding of Manganese to Chloroplast Coupling Factor 1. *Biochemistry*, 20(22) 6287-6292, **1981**.

[3] Rutherford, A. W., Boussac, A. Water Photolysis in Biology. *Sci*., 303, 1782-1784, **2004**.
[4] Constant.G. Lipid Metabolism of Manganese-Deficient Alage.1. Effect of Manganese Deficiency on Greening and Lipid Composition of Euglena gracilis Z. *Plant Physiol.*, 45, 76-80, **1970**.
[5] Lerer, M., Bar-Akiva, A. Nitrogen Constituents in Manganese-Deficient Lemon Leaves. *Physiol. Plant.*, 38, 13-18, **1976**.
[6] Neumann, K. H., Steward, F. C. Investigations on the Growth and Metabolism of Cultured Explants of Daucuscarota. *Planta*, 81, 333-350, **1968**.
[7] Spiller, S. C., Kaufman, L. S., Thompson, W. F., Briggs, W. R. Specific mRNA and rRNA Levels in Greening Pea Leaves during Recovery from Iron Stress. *Plant Physiol.*, 84, 409-414, **1987**.
[8] Dansen, T. B., Wirtz, K. W. A. The Peroxisome in Oxidative Stress.*IUBMB Life*, 51, 223-230, **2001**.
[9] Pankowski, A., McMinn, A. Iron Availability Regulates Growth, Photosynthesis, and Production of Ferredoxin and Flavodoxin in Antarctic Sea Ice Diatoms. *Aquat. Biol.*, 4, 273-288, **2009**.
[10] Iljin, W. S. Metabolism of Plants Aaffected with Lime-Induced Chlorosis (Calciose). *Plant Soil*, 3, 239-256, **1951**.
[11] Aubert, H., Pinta, M. Trace Elements in Soils. *Soil Sci.*, 125, 334, **1978**.
[12] Marton, L. Crop demand of manganese. *Environ.Geochem. Health*, 34, 123-134, **2012**.
[13] Uren, N.C. The Movmement and Distribution of Manganese Added to Soil.*Aust. J. Soil Res.*, 28, 677-683, **1990**.
[14] Welch, R. M., Allaway, W. H., House, W. A., J., K. Geographic Distribution of Trace Element Problems, in *Micronutrients in Agriculture*, J.J. Mortvedt, Editor., Soil Science Society of America: Madison, **1991**.
[15] Neely, D. Iron deficiency chlorosis of shade trees. *J.Arboric.*, 2, 128-130, **1976**.
[16] Walter, K. H. Manganese fertilizers, in *Manganese in Soils and Plants*, R.D. Graham, R.J. Hannam, and N.C. Uren, Editor., Kluwer Academic Publishers. p. 238, **1988**.
[17] Simoglou, K. B., Dordas, C. Effect of foliar applied boron, manganese and zinc on tan spot in winter durum wheat. *Crop Prot.*, 25, 657-663, **2006**.
[18] Papadakis, L. E., Sotiropoulos, T. E., Therios, I. N. Mobility of iron and manganese within two citrus genotypes after foliar applications of iron sulfate and manganese sulfate. *J. Plant Nutr.*, 30, 1385-1396, **2007**.
[19] Dordas, C. Foliar Application of Manganese Increases Seed Yield and Improves Seed Quality of Cotton Grown on Calcareous Soils. *J. Plant Nutr.*,32, 160-176, **2009**.
[20] Movahhedy-Dehnavy, M., Modarres-Sanavy, S. A. M., Mokhtassi-Bidgoli, A. Foliar application of zinc and manganese improves seed yield and quality of safflower (Carthamustinctorius L.) grown under water deficit stress. *Industrial Crops and Products*, 30, 82-92, **2009**.
[21] Haslett, B. S., Reid, R. J., Rengel, Z. Zinc Mobility in Wheat: Uptake and Distribution of Zinc Applied to Leaves or Roots. *Ann. Bot.*, 87, 379-386, **2001**.
[22] Shaviv, A. Advances in controlled-release fertilizers, in *Advances in Agronomy*., Academic Press. 77 1-49, **2001**.
[23] Heenan, D. P., Campbell, L. C. Manganese and Iron Interactions on Their Uptake and Distribution in Soybean (Glycine-Max (L) Merr). *PlantSoil*, 70, 317-326, **1983**.
[24] Nable, R. O., Barakiva, A., Loneragan, J. F. Functional Manganese Requirement and Its Use as a Critical Value for Diagnosis of Manganese Deficiency in Subterranean Clover (Trifolium- Subterraneumlcv Seaton Park). *Ann. Bot.*, 54, 39-49, **1984**.
[25] Nable, R. O., Houtz, R. L., Cheniae, G. M. Early Inhibition of Photosynthesis During Development of Mn Toxicity in Tobacco. *Plant Physiol.*, 86, 1136-1142, **1988**.
[26] Kohno, Y., Foy, C. D. Manganese Toxicity in Bush Bean as Affected by Concentration of Manganese and Iron in the Nutrient Solution. *J. Plant Nutr.*, 6, 363-386, **1983**.
[27] El-Jaoual, T., Cox, D. A. Manganese toxicity in plants. *J. Plant Nutr.*,21, 353-386, **1998**.
[28] Bridger, G. L., Salutsky, M. L., Starostka, R. W. Micronutrient Sources, Metal Ammonium Phosphates as Fertilizers. *J. Agri. Food Chem.*, 10, 181-188, **1962**.
[29] Xu, X., Shi, J., Chen, X., Chen, Y., Hu, T. Chemical forms of manganese in the leaves of manganese hyperaccumulator Phytolaccaacinosa Roxb. (Phytolaccaceae).*Plant Soil*, 318, 197-204, **2009**.
[30] Angermann, A., Topfer, J. Synthesis of Magnetite Nanoparticles by Thermal Decomposition of Ferrous Oxalate Dihydrate. *J. Mat. Sci*., 43, 5123-5130, **2008**.
[31] Danvirutai, C., Noisong, P., Youngme, S. Some thermodynamic functions and kinetics of thermal decomposition of $NH_4MnPO_4{\bullet}H_2O$ in nitrogen atmosphere.*J. Therm. Anal..Calorim.*, 100, 117-124, **2010**.
[32] Malecka, B., Drozdz-Ciesla, E., Olszewski, P. Kinetics of thermal decomposition of manganese(II) oxalate. *J.Therm. Anal..Calorim.*, 74, 485-490, **2003**.
[33] Mancilla, N., Caliva, V., D'Antonio, M. C., González-Baró, A. C., Baran, E. J. Vibrational spectroscopic investigation of the hydrates of manganese(II) oxalate. *J. of Raman Spectrosc*., 40, 915-920, **2009**.
[34] D'Antonio, M. C., Wladimirsky, A., Palacios, D., Coggiolaa, L., González-Baró, A. C., Baran, E. J., Mercader, R. C. Spectroscopic investigations of iron(II) and iron(III) oxalates. *J. Braz.Chem.Soc.*, 20, 445-450, **2009**.
[35] Alfonso, B. F., Trobajo, C., Pique, C., Garcia, J. R., Blanco, J. A. From dihydratediron(III) phosphate to monohydrated ammonium-iron(II) phosphate: Solvothermal reaction mediated by acetone-urea mixtures. *J. Solid State Chem.*, 196, 458-464, **2012**.
[36] Koga, N., Sato, Y. Formation and Transformation Kinetics of Amorphous Iron(III) Oxide during the Thermally Induced Transformation of Ferrous Oxalate Dihydrate in Air. *J. Phys. Chem. A*, 115, 141-151, **2011**.
[37] LaMer, V. K., Dinegar, R. H. Theory, Production and Mechanism of Formation of Monodispersed Hydrosols. *J. Am. Chem. Soc.*, 72, 4847-4854, **1950**
[38] Glusker, J. P. Citrate conformation and chelation: enzymic implications. *Acc. Chem. Res.*, 13, 345-352, **1980**.
[39] Chemical Rubber, C. *Handbook of chemistry and physics: a ready-reference pocket book of chemical and physical data*, Cleveland, Ohio: CRC Press, **2004**.
[40] *Ferrous Ammonium Phosphate Gras Notice*. Nestle USA, Inc., **2008**.
[41] Römheld, V., Marschner, H. Function of Micronutrients in Plants, in *Micronutrients in agriculture*, J.J. Mortvedt, Editor., Soil Science Society of America: Madison, **1991**.
[42] Horst, W. J. The Physiology of Manganese Toxicity, in *Manganese in Soils and Plants*, R.D. Graham, R.J. Hannam, and N.C. Uren, Editors., Kluwer Academic Publishers: Dordrecht , Boston , London, **1988**.

5. ACKNOWLEDGEMENTS

This research was supported under Australian Research Council's Linkage Projects funding scheme (project number LP0989217) and Australian Research Council's Future Fellowship (FT120100813). The information reported in this paper has been covered by the Australian Patent 2011900756.